Simulation of wrinkling during textile composite reinforcement forming. Influence of tensile, in-plane shear and bending stiffnesses

P. Boisse, N. Hamila, E. Vidal-Sallé, F. Dumont

Simulation of wrinkling during textile composite reinforcement forming. Influence of tensile, in-plane shear and bending stiffnesses

P. Boisse, N. Hamila, E. Vidal-Sallé, F. Dumont

PII: S0266-3538(11)00039-X
DOI: 10.1016/j.compscitech.2011.01.011
Reference: CSTE 4906

To appear in: *Composites Science and Technology*

Received Date: 13 May 2010
Revised Date: 10 January 2011
Accepted Date: 16 January 2011

Please cite this article as: Boisse, P., Hamila, N., Vidal-Sallé, E., Dumont, F., Simulation of wrinkling during textile composite reinforcement forming. Influence of tensile, in-plane shear and bending stiffnesses, *Composites Science and Technology* (2011), doi: 10.1016/j.compscitech.2011.01.011

Simulation of wrinkling during textile composite reinforcement forming. Influence of tensile, in-plane shear and bending stiffnesses

P. Boisse[1]*, N. Hamila[1], E. Vidal-Sallé[1], F. Dumont[2]

[1]Université de Lyon, INSA-Lyon, LaMCoS, F-69621, France

[2]Eurocopter Deutschland GmbH, Lab. for Materials & Processes, D-81663 Munich, Germany

Abstract

Wrinkling is one of the most common flaws that occur during textile composite reinforcement forming processes. These wrinkles are frequent because of the possible relative motion of fibres making up the reinforcement, leading to a very weak textile bending stiffness. It is necessary to simulate their onset but also their growth and their shape in order to verify that they don't extend to the useful part of the preform. In this paper the simulation of textile composite reinforcement forming and wrinkling is based on a simplified form of virtual internal work defined according to tensions, in-plane shear and bending moments on a unit woven cell. The role of the three rigidities (tensile, in-plane shear and bending) in wrinkling simulations is analysed. If in-plane shear stiffness plays a main role for onset of wrinkles in double-curved shape forming, there is no direct relation between shear angle and wrinkling. Wrinkling is a global phenomenon depending on all strains and stiffnesses and on boundary conditions. The bending stiffness mainly determines the shape of the wrinkles and it is not possible to perform a wrinkle simulation using a membrane approach.

Key words: Fabrics/textiles (A), Finite element analysis (C), Buckling (C), Resin transfer moulding (RTM) (E), Wrinkling

1 - Introduction

To manufacture textile composite double-curved components, draping of pre-impregnated or dry textile sheets is required. In the case of dry reinforcement, a liquid composite moulding (LCM) process is applied, which consists of the impregnation of the formed reinforcement

* Corresponding author. Tel.: +33 4 72 43 63 96; E-mail address: philippe.boisse@insa-lyon.fr

and the consolidation of the resin [1, 2]. Textile reinforcement deformation can be significant. In particular, large in-plane shear could be necessary to obtain the required shape. Depending on part geometry, reinforcement type (weaving, material...) and on manufacturing parameters (tool loads, blank holder…), double-curved shapes may contain defects. Simulation software for composite forming has been developed to determine the process feasibility parameters [3-6]. Among the defects that occur during textile reinforcement forming process, wrinkles are the most common ones. These wrinkles develop easily because of the internal composition of textile reinforcement made out of fibres. Possible relative fibre motions result in a specific mechanical behaviour that characterizes very low bending stiffness creating favourable conditions for wrinkles.

Wrinkling is a major issue to be addressed in designing thin parts and forming parameters of sheet forming. Much research efforts have been made to predict wrinkling of isotropic [7-10] and anisotropic sheets [11, 12]. In case of composite textile reinforcements, the internal structure of the fabric made of yarns and fibres makes the wrinkling phenomenon specific and frequent. Some in-plane shear experimental studies have analysed wrinkling focusing on the shear locking angle as onset of wrinkle condition [13-18]. Numerical analysis of onset of wrinkling has been proposed, mainly based on kinematic models (also called fishnet algorithms) [19-21], simplified truss representations [22] or membrane approaches of the woven material [23-25].

This paper considers a simplified form of the internal virtual work in the case of textile composite reinforcements. Tensile, in-plane shear and bending virtual works are separated and added on a unit woven cell. The form of these virtual works is simple and close to textile material physics. The involved material data are directly identified through mechanical tests performed for the case of textile reinforcements. The mechanical tests include biaxial tests for tensile stiffness [26-29], picture frame and bias-extension tests for in-plane shear stiffness [13-18, 30-36] and bending tests [37-39]. This approach avoids determination of the material properties within the framework of a continuous mechanical approach [40-43].

A three node shell finite element for fabric forming simulations is based on this form of the internal virtual work [44, 45]. It is used to simulate textile reinforcements draping and forming processes and to analyse the onset and growth of wrinkles as a function of the three stiffnesses (tension, in plane shear and bending)

Wrinkling can be due to compression in the yarn direction (this is usually avoided in forming process) or to large in plane shear strains. The in-plane shear stiffness of a fabric strongly increases when the shear angle becomes large, especially when it reaches and exceeds the 'locking angle'. Nevertheless wrinkling is a global phenomenon that depends on the set of all strains and stiffnesses. The example presented in section 5.5 shows that there is no simple relation between the shear angle and wrinkling. Especially tensions (created by blank holders) can avoid wrinkling even for very large shear angle.

Bending stiffness plays an important role in the wrinkle shape. An increase of this rigidity leads to an increase of the wrinkle size. For some forming processes, there are zones where wrinkles cannot be avoided. In these cases it is important to simulate the shapes of these wrinkles in order to check they do not expand to the useful part of the preform. This is not possible for membrane approaches (no bending stiffness) that are common in textile sheet forming simulation. The examples of section 5 show that an effective simulation of wrinkling needs to take tensions, in-plane shear and bending strain energies into account.

2 – Mechanical behaviour of textile composite reinforcements

2.1. – Load resultants on a unit woven cell

The textile composite reinforcement consists of woven unit cells. Its mechanical behaviour is specific because of the possible relative displacements between yarns and between fibres within the yarns. Let's consider the loads on a unit woven cell (RUC= Representative Unit Cell) such as Fig. 1a. The following resultants of these loads are considered:

- The tensions T_1 and T_2 are the resultants of the loads respectively on warp and weft yarns in the directions $\underline{f}_1$ and $\underline{f}_2$ of these yarns (Fig. 1b)

- The in-plane shear moment M_s is the moment at the centre of the RUC, in the direction of the normal to the fabric, resulting from the in-plane loads on the unit woven cell (Fig. 1c).

- The bending moments M_1 and M_2 resulting on the warp and weft yarns (Fig. 1d).

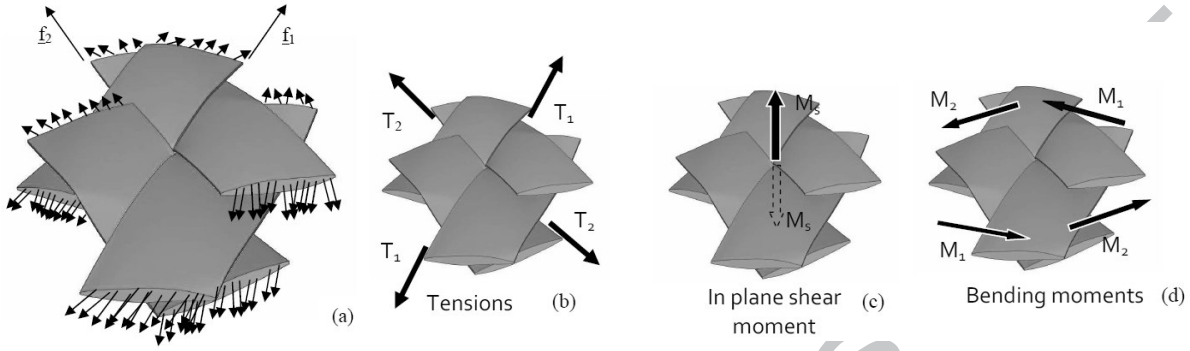

Fig. 1. (a) Loads on a unit woven cell and resultants:
(b) tensions, (c) in-plane shear moment, (d) bending moments.

It will be considered that the loading on the unit woven cell is characterized by these load resultants T_1, T_2, M_s, M_1 and M_2. This is a simplified modelling, but physical meanings of these quantities are clear. Furthermore these loads are directly measured as functions of the deformation of the fabric in standard tests for composite reinforcements (see sections 2.3 to 2.5). Finally these loads T_1, T_2, M_s, M_1 and M_2 are conjugated respectively to axial strains ε_{11}, ε_{22} in warp and weft directions, to in-plane shear angle γ, and to curvatures χ_{11} and χ_{22} of warp and weft yarns. Consequently this leads to the simple form of the internal virtual work presented below.

2.2. – Principle of virtual work

A textile composite reinforcement is made of N_c unit woven cells such as shown in Fig. 1. These figures have been drawn in the case of a plain weave for simplicity but the type of weaving can be different (twill, satin…). The principle of virtual work can be written:

$$\forall \underline{\eta} / \underline{\eta} = 0 \text{ on } \Gamma_u, \qquad W_{ext}(\underline{\eta}) - W_{acc}(\underline{\eta}) =$$

$$\sum_{p=1}^{N_c} {}^{p}\underbrace{\varepsilon_{11}(\underline{\eta})\ {}^{p}T_1\ {}^{p}L_1 + {}^{p}\varepsilon_{22}(\underline{\eta})\ {}^{p}T_2\ {}^{p}L_2}_{(b)} + \underbrace{\gamma(\underline{\eta})\ {}^{p}M_s}_{(c)} + \underbrace{{}^{p}\chi_{11}(\underline{\eta})\ {}^{p}M_1\ {}^{p}L_1 + {}^{p}\chi_{22}(\underline{\eta})\ {}^{p}M_2\ {}^{p}L_2}_{(d)} \tag{1}$$

$W_{ext}(\underline{\eta})$ and $W_{acc}(\underline{\eta})$ are respectively the virtual work of the exterior loads and the virtual work of the acceleration quantities in the virtual displacement field $\underline{\eta}$ ($\underline{\eta}$ is equal to zero on

the boundary with prescribed displacements Γ_u). The quantity A is denoted ${}^pA$ when it concerns the unit woven cell number p. Part (b) of the internal virtual work is due to tensions. $\varepsilon_{11}(\underline{\eta})$ and $\varepsilon_{22}(\underline{\eta})$ are the virtual axial strains in warp and weft directions. L_1 and L_2 are the lengths of the unit cell in warp and weft directions. Part (c) is the internal virtual work due to in-plane shear. $\gamma(\underline{\eta})$ is the virtual angle variation between warp and weft directions in the displacement field $\underline{\eta}$. Part (d) is the internal virtual work due to bending. $\chi_{11}(\underline{\eta})$ and $\chi_{22}(\underline{\eta})$ are the virtual curvatures in warp and weft directions. The virtual strains $\varepsilon_{11}(\underline{\eta})$, $\varepsilon_{22}(\underline{\eta})$, $\gamma(\underline{\eta})$, $\chi_{11}(\underline{\eta})$ and $\chi_{22}(\underline{\eta})$ are function of the virtual displacement field $\underline{\eta}$.

Remark 1. Equation 1 and wrinkling analysis

The form of the principle of virtual work written in equation (1) is suitable to analyse the role of the three stiffnesses in wrinkle formation. The virtual works of tension (b) in-plane shear (c) and bending (d) will be considered in turn in the forming analyses presented in section 5 to outline their respective and combined effect.

Remark 2, concerning the in-plane shear moment:

In the case of textile deformation, the shear angle γ (i.e. the angle variation between warp and weft yarns) is a significant and clearly defined quantity. It is used in all the studies concerning in-plane shear behaviour of textile reinforcement (see section 2.3). It is interesting to express the internal virtual work of in-plane shear as a function of this quantity. The load conjugated to this shear angle is the moment M_s (Equation 1c). As defined above, it is the component in the normal direction of moment at the centre of the RUC due to the loads on the yarns (Fig. 1c).

Remark 3. concerning the load resultants:

Defining the loading state on a woven unit cell by the load resultants T_1, T_2, M_s, M_1, M_2 is a simplified modelling. Nevertheless, we believe that it is better fitted to describe the load state in a textile than a standard stress field. This stress tensor $\underline{\underline{\sigma}}$ defines a load $\underline{T}$ on an elementary surface according to its normal $\underline{n}$ ($\underline{T} = \underline{\underline{\sigma}}.\underline{n}$). In the case of textile materials, the surfaces and

consequently, the normal vectors are not all well defined and the stress definition is questionable.

Remark 4, concerning the twisting curvature:

In addition to equation 1d, the bending virtual work should include $\chi_{12}(\underline{\eta})\, M_{12}$ coming from the twisting curvature. This term is neglected in the present approach mainly because of the lack of experimental data. Nevertheless this twisting term is probably small in case of woven material because of the structure of the fabric made of two warp and weft sets of yarns.

The load resultants T_1, T_2, M_s, M_1, M_2 depend on the strains in the textile material. The next sections (2.3 to 2.5) briefly describe the experiments used to characterize the mechanical behaviours, i.e. the relations between the load resultants T_1, T_2, M_s, M_1, M_2 and the strains in the material. These experiments are specific to textile composite reinforcements.

2.3. – In-plane shear behaviour

Two experimental tests are used to determine the in-plane shear behaviour of textile composite reinforcements: the picture-frame (Fig. 2) and the bias-extension tests (Fig. 3). A great amount of literature is dedicated to those tests [13-18, 30-36] mainly because the in-plane shear is the most dominant deformation mode in woven composite forming when the manufactured part is doubly curved. The shear angle can reach 50° (and even more in some cases such as presented in section 5.5). For large values, wrinkling can occur depending on the process parameters and on the material properties. In addition, the two tests are difficult both from the experimental point of view and concerning the interpretation of the results. For these reasons an international benchmark has been launched recently. Eight laboratories of six different countries have performed picture frame and bias-extension tests on the same textile composite reinforcements [36].

The picture-frame (or trellis-frame) is made of four hinged bars (Fig. 2). The fabric specimen is initially square and the tows are parallel to the bars. Consequently it is theoretically subjected to pure in-plane shear. The shear angle for a given displacement d is :

$$\gamma = \frac{\pi}{2} - 2\arccos\left(\frac{1}{\sqrt{2}} + \frac{d}{2L}\right) \quad (2)$$

The power P provided by the traction machine and the power absorbed by the sheared fabric are assumed to be equal ($\dot{d}$ is the speed of the machine, S_u is the surface of a unit woven cell in the initial configuration, L is the width of the specimen) :

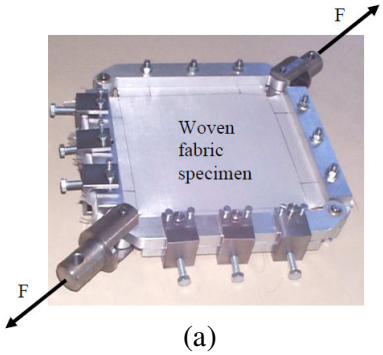

(a)

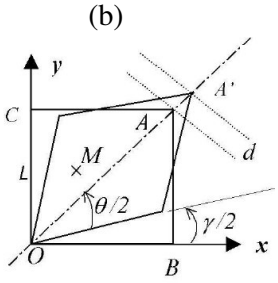

(b)

$$P = F(\gamma)\dot{d} = \frac{L^2}{S_u} M_s(\gamma)\dot{\gamma} \quad (3)$$

Taking the geometry of the frame into account :

$$M_s(\gamma) = F(\gamma)\frac{S_u}{\sqrt{2}L}\left(\cos\frac{\gamma}{2} - \sin\frac{\gamma}{2}\right) \quad (4)$$

Fig. 2. Picture frame test. (a) Experimental device. (b) Kinematics of the test

The bias-extension test is an alternative to the picture-frame test. It consists of clamping a rectangular specimen of woven fabric with warp and weft directions initially oriented at 45° with respect to the tensile load applied by a tensile machine (Fig 3.). The initial length of the specimen L must be larger than twice the width ℓ. The zone C in the centre of the specimen is submitted to a pure shear γ if the yarns are assumed to be inextensible. That is a correct assumption for the type of yarns used as composite reinforcements. This inextensibility imposes that the shear angle in the zone B is half the value in the central region C.

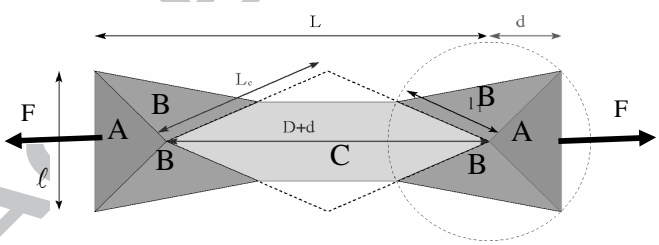

Fig. 3. The three zones of the bias-extension test

$$\gamma = \frac{\pi}{2} - 2\arccos\left(\frac{D+d}{\sqrt{2}D}\right) \quad (5)$$

The power made through the clamping force, F, is dissipated in the zones B and C.

Denoting S_b and S_c the original area of zone B and C [34, 36]:

$$F(\gamma)\dot{d} = M_s(\gamma)\frac{S_C}{S_u}\dot{\gamma} + M_s\left(\frac{\gamma}{2}\right)\frac{S_B}{S_u}\frac{\dot{\gamma}}{2} \quad (6)$$

From the geometry of the specimen this leads to:

$$M_s(\gamma)=\frac{F(\gamma)DS_u}{\ell\left(2D-\ell\right)}\left(\cos\frac{\gamma}{2}-\sin\frac{\gamma}{2}\right)-\frac{\ell}{2D-\ell}M_s\left(\frac{\gamma}{2}\right) \quad (7)$$

A shear curve $M_s(\gamma)$ measured in the case of glass plain weave is presented in Fig. 4. In the first part of the curve (i.e. for small shear angles), the in-plane shear stiffness is small.

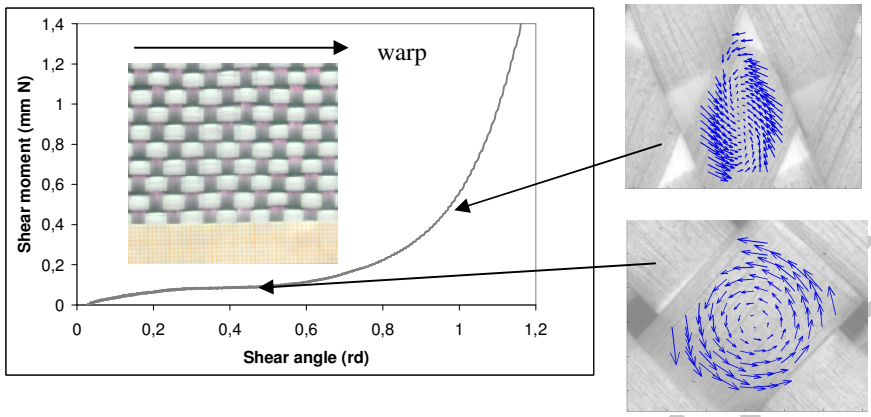

Fig. 4.(a) Shear curve of glass plain weave, (b) relative displacement field inside a yarn

For larger shear angles this rigidity increases and becomes significant. The optical field measurements performed within the tow show that during the first part of the loading, the tows rotate in a rigid body motion (Fig 4b). When the shear angle becomes larger lateral contacts between the yarns occur [35]. The tows are progressively compressed and the shear rigidity increases significantly. This increase of shear stiffness leads to wrinkling onset. The corresponding shear angle is called the locking angle (in order of 40°- 45° for textile composite reinforcements [13, 36]).

2.4. – Biaxial tensile behaviour

The tensile behaviour of woven material is specific mainly because of the decrimping of tows when they are stretched. This leads to tensile behaviour non-linearities. The fabric is much softer than the tow for small axial strains. Because of the weaving, the decrimping phenomenon in warp and weft directions are interdependent and the tensile behaviour is biaxial. Some biaxial tests have been developed in order to measure these properties [26-29]. Fig. 5 shows a biaxial tensile device using a cross shape specimen [47].

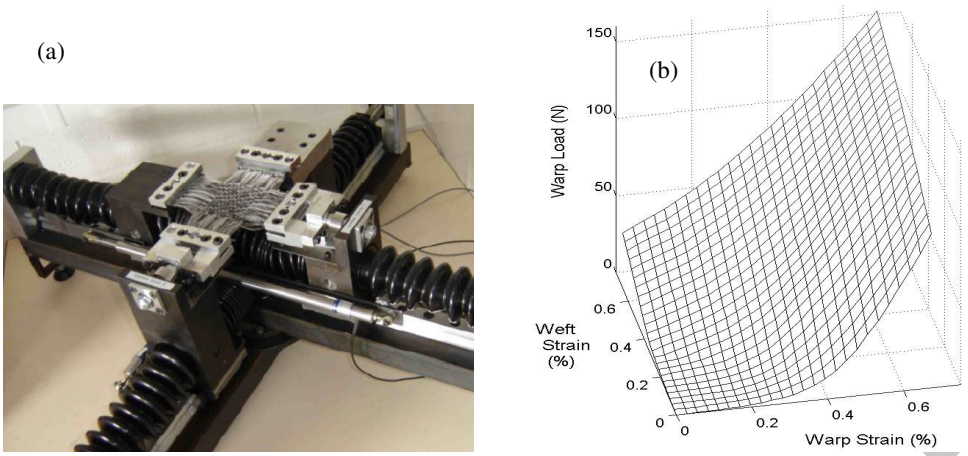

Fig. 5 (a) Biaxial tensile device and (b) Biaxial tensile surface

The measurements of tensions in warp and weft directions give two tensile surfaces $T_1(\varepsilon_{11}, \varepsilon_{22})$ and $T_2(\varepsilon_{11}, \varepsilon_{22})$ (Fig 5b. in the case of the balanced glass plain weave presented Fig. 4.) It has been experimentally shown that the influence of the shear angle on the tensile behaviour is usually weak and can be neglected [27].

2.5. – Bending behaviour

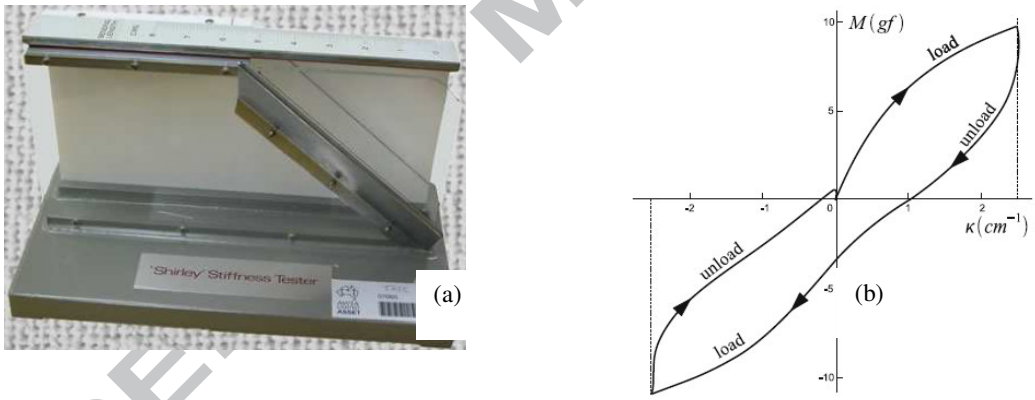

Fig. 6. (a) ASTM, Standard test method for bending stiffness of fabrics [48],
(b) A representative bending test result [39]

The bending stiffness of textile sheets is very weak in comparison with continuous materials such as sheet metal or composite plates with hardened matrix. This is due to the possible relative motions of fibres. Consequently the relation given by the plate theory between the tensile and the bending stiffnesses is no longer valid. The tensile rigidities are so large in comparison with bending ones that a membrane assumption is often made for fabric deformation simulations. Nevertheless it will be shown in the examples presented below that the bending stiffness is important in wrinkling simulations.

Two main devices are used for the measurement of woven fabric bending properties. The KES-FB system [37] and the ASTM cantilever bending device developed from the work of Peirce [48, 49, 39] (Fig. 6a). In this test the fabric is cantilevered under gravity. The bending moment at the clamping section due to the weight of the fabric is related to the curvature calculated from the geometry of the specimen (Fig 6b).

In the present work only the bending moments in the warp and weft directions are taken into account and they are assumed to only depend respectively on warp and weft curvatures

3 – Shell finite element made of woven cells

The three node shell finite element used in this paper is based on the simplified form of the principle of virtual works given in equation 1. The details of its formulation are given in [44, 45]. It is summarized below. The tensile, in-plane shear and bending internal loads are separated in order to analyse their influence on wrinkling simulations.

3.1. Dynamic equation and central difference scheme

A finite element interpolation is introduced within the principle of virtual work (1). The displacement $\underline{u}$ and virtual displacement $\underline{\eta}$ of any point within an element is in the form:

$$\underline{u} = \mathbf{N}\mathbf{u}^e \qquad \text{and} \qquad \underline{\eta} = \mathbf{N}\boldsymbol{\eta}^e \tag{8}$$

$\mathbf{N}$ is the interpolation matrix of the element under consideration and $\mathbf{u}^e$ and $\boldsymbol{\eta}^e$ the single column matrices of its nodal displacements and virtual displacements respectively. Equation 1 leads to:

$$\mathbf{M}\ddot{\mathbf{u}} + \left(\mathbf{F}_{int}^{t} + \mathbf{F}_{int}^{s} + \mathbf{F}_{int}^{b}\right) - \mathbf{F}_{ext} = 0 \tag{9}$$

$\mathbf{M}$ is the mass matrix, $\mathbf{u}$ is the single column matrix of the nodal displacements. $\mathbf{F}_{int}^{t}, \mathbf{F}_{int}^{s}, \mathbf{F}_{int}^{b}$ are the single column matrices of the nodal internal forces respectively for tension, shear and bending.

This dynamic equation can be solved using an explicit scheme (central differences):

$$\ddot{\mathbf{u}}^{i+1} = \mathbf{M}_D^{i\,-1}\left(\mathbf{F}_{ext}^{i} - \mathbf{F}_{int}^{ti} - \mathbf{F}_{int}^{si} - \mathbf{F}_{int}^{bi}\right), \qquad \dot{\mathbf{u}}^{i+1/2} = \dot{\mathbf{u}}^{i-1/2} + \frac{1}{2}\left(\Delta t^{i-1} + \Delta t^{i}\right)\ddot{\mathbf{u}}^{i+1}, \qquad \mathbf{u}^{i+1} = \mathbf{u}^{i} + \dot{\mathbf{u}}^{i+1/2}\Delta t^{i} \tag{10}$$

There is no system to solve since $\mathbf{M}_D$ is a diagonal matrix calculated from $\mathbf{M}$ [50]. This explicit scheme requires the time step to be small enough to insure the stability of the scheme [51]. It is effective for many dynamic applications and also in material forming. For the sake of numerical efficiency, the speed can be larger than the real one under the condition that the dynamic effects do not modify the solution.

This explicit dynamic approach presents an advantage concerning the wrinkle simulation. The acceleration term in equation (9) avoids the instability that occurs with buckling in a quasi static approach. The wrinkle development shown in the examples presented in section 5 are directly simulated using the above explicit scheme. In the numerical scheme (10) the only quantities depending on the material properties are the nodal internal forces.

3.2. Internal nodal forces

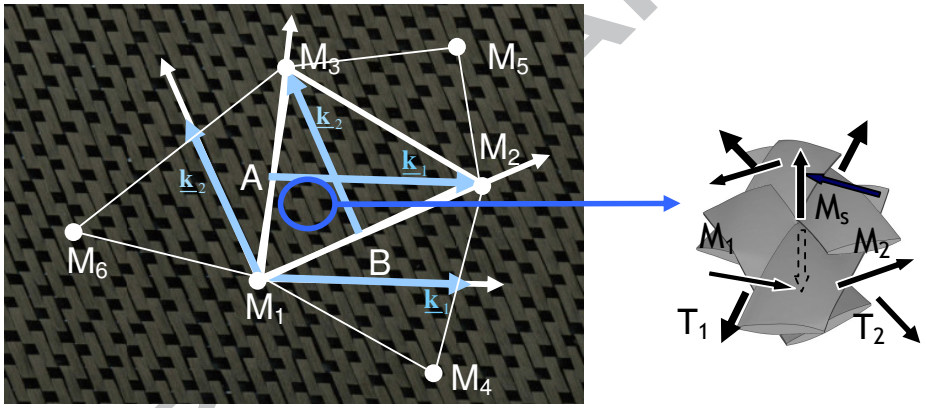

Fig. 7. Three node finite element made of unit woven cells,

A 3 node shell finite element $M_1M_2M_3$ made up of ncelle woven cells is considered (Fig. 7). The vectors $\underline{k}_1=\underline{AM}_2$ and $\underline{k}_2=\underline{BM}_3$ respectively in warp and weft directions are defined. The internal virtual work of tension on the element (part (b) in equation 1) defines the element nodal tensile internal forces $\mathbf{F}_{int}^{te}$:

$$\sum_{p=1}^{ncelle} {}^{p}\varepsilon_{11}(\underline{\eta})\ {}^{p}T_1\ {}^{p}L_1 + {}^{p}\varepsilon_{22}(\underline{\eta})\ {}^{p}T_2\ {}^{p}L_2 = \boldsymbol{\eta}^{eT}\mathbf{F}_{int}^{te} \tag{9}$$

The internal tensile force components are calculated from the tensions T_1 and T_2:

$$\left(F_{int}^{te}\right)_{ij} = ncelle\left(B_{1ij}T_1\frac{L_1}{\|\underline{k}_1\|^2} + B_{2ij}T_2\frac{L_2}{\|\underline{k}_2\|^2}\right) \tag{10}$$

i is the index of the direction (i=1 to 3), j is the index of the node (j=1 to 3). B_{1ij} and B_{2ij} are strain interpolation components. They are constant over the element because the interpolation functions in equation 8 are linear in the case of the 3 node triangle.

The internal virtual work of in-plane shear on the element (part (c) in equation 1) defines the element nodal tensile internal forces $\mathbf{F}_{int}^{se}$:

$$\sum_{p=1}^{ncelle} {}^{p}\gamma(\underline{\eta})\ {}^{p}M_s = \boldsymbol{\eta}^{eT}\mathbf{F}_{int}^{se} \tag{11}$$

The internal in-plane shear force components are calculated from the in-plane shear moment:

$$\left(F_{int}^{se}\right)_{ij} = ncelle\ B_{\gamma ij} M_s\left(\gamma\right) \tag{12}$$

In order to avoid supplementary degrees of freedom and consequently for numerical efficiency, the bending stiffness is taken into account within an approach without rotational degree of freedom [52, 53]. In these approaches the curvatures of the element are computed from the positions and displacements of the nodes of the neighbouring elements (Fig. 7). The internal virtual work of bending on the element (part (d) in equation 1) defines the element nodal bending internal forces $\mathbf{F}_{int}^{be}$:

$$\sum_{p=1}^{ncelle} {}^{p}\chi_{11}(\underline{\eta})\ {}^{p}M_1\ {}^{p}L_1 + {}^{p}\chi_{22}(\underline{\eta})\ {}^{p}M_2\ {}^{p}L_2 = \boldsymbol{\eta}^{eT}\mathbf{F}_{int}^{be} \tag{13}$$

The internal bending force components are calculated from the bending moments M_1 and M_2:

$$\left(F_{int}^{be}\right)_{km} = n_{celle}\left(Bb_{1km} M_1 \frac{L_1}{\left\|\underline{k}_1\right\|^2} + Bb_{2km}\, M_2 \frac{L_2}{\left\|\underline{k}_2\right\|^2} \right) \tag{14}$$

3.3 Remark concerning 'shear locking'.

In recent years, there has been some debate on intra-ply shear locking [54, 55]. The finite elements for fabric forming simulation can lock (i.e. give a too stiff numerical result) if the fibres are not aligned with the element edges. In the present work fibres are edge-aligned in order to avoid this difficulty. This is possible because of the rectangular shapes of the fabrics.

4 –**Wrinkling in textile composite reinforcement forming**

The present study concerns forming of thin textile composite reinforcements (so called 2D reinforcements). The thickness is small in relation to the warp and weft lengths. Consequently, the wrinkling risk is high and strongly increased by the fibrous nature of the reinforcement. Thin structures are subject to wrinkling as their bending stiffness is much lower than the in-plane (membrane) one. For a given thickness, the bending stiffness of a woven fabric is lower than one of a plate made of a continuous material because of the possible sliding between its constituting fibres. The ability to develop wrinkles is thus very high for textile materials. Wrinkles are numerous in many forming processes, and the identification of the forming parameters avoiding those wrinkles in the useful part of the mechanical component is a key point.

The tendency to generate out of plane deformation or wrinkle is a function of lower energy dissipation compared to in plane deformation. As a result the compression during forming process manifests itself as wrinkle (see section 5.1). The wrinkle increases the fabric length, therefore the strain energy corresponding to compression decreases. It is noted that in industrial settings compression (and thus wrinkles) can be prevented with the addition of forming constraints such as blank holders. These constraints apply a tension to the fibres which works to reduce the formation of wrinkles.

In the case of fibrous reinforcements doubly curved shapes are obtained thanks to in-plane shear i.e. angle changes between warp and weft yarns. It is the primary mechanism of the textile forming. It uses the low in-plane shear rigidity (in comparison with the yarn tensile one). Nevertheless, when the shear angles become high (for example >40° for classical reinforcements), the shear stiffness increases because lateral contact occurs between adjacent yarns (Fig. 4.). A deformed shape of the fabric with wrinkles can lead to a decrease of the shear angles. The bending strain energy linked to the increase of curvatures due to wrinkling remains small with respect to in-plane shear strain energy. This leads generally to wrinkle onset for shear angles larger than the so-called locking angle. This locking angle has been highlighted from in plane shear experimental tests, especially picture frame tests [13-18]. In

these tests, the onset of wrinkles correspond to an angle of the frame which is called 'locking angle' and is considered in many works as a characteristic value for describing the potential of the fabric to be formed on a double curved surface. Some forming analyses and especially those based on kinematical methods compare the shear angle given by the draping simulations to the locking angle [19-21]. They conclude that there are wrinkles in the zone with shear angle larger than the locking angle.

Nevertheless wrinkling is a global phenomenon and there is no simple relation between the shear angle and the wrinkles. Wrinkles are due to all strains and rigidities of the fabric (tension, in-plane shear and bending) and to boundary conditions. A blank holder can increase the tensions and consequently avoid wrinkling.

The examples presented in section 5 confirm that in-plane shear strain state and rigidities are the main factor of wrinkling onset during a forming process. In addition it can be important to compute the shape of the wrinkles after forming in order to check that these wrinkles do not extend to the useful part of the preform. Many forming simulations are based on membrane approaches (no bending stiffness) [22-25 40-43]. It is shown in the next section that such a membrane assumption leads to a very large number of small wrinkles. The bending stiffness is necessary to compute the actual geometry of the wrinkles. When this bending stiffness increases, the wrinkle size increases too (and their number decreases). It is necessary to take the bending stiffness into account in order to check that the wrinkle do not extend to the useful part of the preform.

5 –Simulation examples. Analysis of the influence of tensile, in-plane shear and bending rigidities on wrinkling

The properties of the textile reinforcement considered in the different following examples are given in table 1. The friction coefficient is f = 0.2 in all these examples. The speed of the forming in the simulation is larger than the real one but it is checked that the kinematical

energy remains small enough to consider that the transformation is quasi-static. The size of the elements must be small enough in order to describe the wrinkles correctly.

5.1. Wrinkling in compression

Textile reinforcements are very sensitive to in plane compression loadings. Their very weak bending stiffness leads to buckling for small compression loads. When a woven fabric is submitted to compression in the yarn direction it tends to an out-of-plane deformation if this one is possible. The bending strain energy induced by this out-of-plane deformation is much smaller than the decrease of compression strain energy.

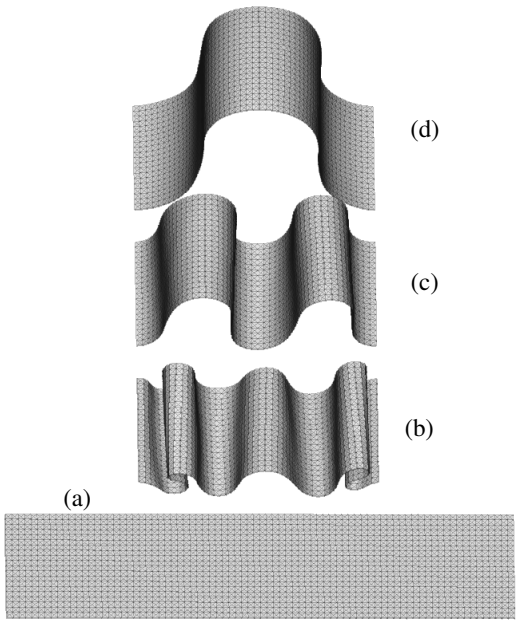

Fig. 8. Compressive deformation for different bending rigidities

A fabric strip is considered Fig. 8a. The two edges of the fabric are moved closer. The prescribed displacement is 42.6 mm. Figures 8b,c,d show the deformed shape obtained for different bending rigidities (respectively 10, 10^2, 10^3 Nmm). The size of the wrinkles increases with the bending stiffness. If the textile reinforcements are very sensitive to compression state for which buckling is quasi immediate, this situation is generally avoided in forming processes. Some tools such as blank holders are used in order to apply tensions and avoid compressive states in the fabric.

	Initial dimensions of the fabric (in mm)	Tensile stiffnesses (in N)	In plane shear stiffness (in Nmm)	Bending stiffnesses (in Nmm)
Test 5.1	80 x 20	3000 (warp and weft)	1000	(8b) 10 (8c) 100 (8d) 1000
Test 5.2	150 x 150	1020 (warp and weft)	$M_s(\gamma) = 0.370\gamma - 0.841\gamma^3 + 1.031\gamma^5$	(9d) 0.51
Test 5.3	330 x 330	50 (warp) 0.2 (weft)	$\begin{cases} M_s(\gamma) = 0.031\gamma \quad \text{if} \quad \gamma \le 0.51\,\text{rd} \\ M_s(\gamma) = 0.095(\gamma - \gamma_c) + 0.031\gamma_c \quad \text{if} \quad \gamma > 0.51\,\text{rd} \end{cases}$	0.102
Test 5.4	400x400	1020 (warp and weft)	$M_s(\gamma) = 0.370\gamma - 0.841\gamma^3 + 1.031\gamma^5$	(11c) 0.15 (11d) 1.5
Test 5.5	900x1000	2300 (warp and weft)	$M_s(\gamma) = 0.371\gamma + 0.416\gamma^3 + 2.428\gamma^5$	(12b) 0.504

Table 1. Geometries and rigidities of the fabric blank in the tests presented in section 5.

5.2 Draping on an hemisphere

The draping of a woven reinforcement on a hemisphere is considered (Fig. 9). The first deformed shape (Fig. 9b) is obtained only accounting for the tensile part (b) in the virtual internal work of equation (1). The draping is perfectly obtained without any wrinkle but the shear angles near the corners of the fabric are close to 90°. The obtained solution is similar to the one given by a fishnet algorithm. Only the axial strains due to tensions in the yarns can lead to a difference. But these strains are very small in the present case because there are very weak tensions during the draping. The second deformed shape (Fig 9c) is obtained when the tension (b) and in-plane shear (c) parts are taken into account in the virtual internal work of equation (1). The draping is performed but wrinkles appear. Those wrinkles are numerous and small. The third deformed shape (Fig 9d) is obtained when all the terms (tension (b), in-plane shear (c) and bending (d)) are taken into account. In this case too, the draping leads to wrinkles but they are less numerous and the deformed shape is realistic.

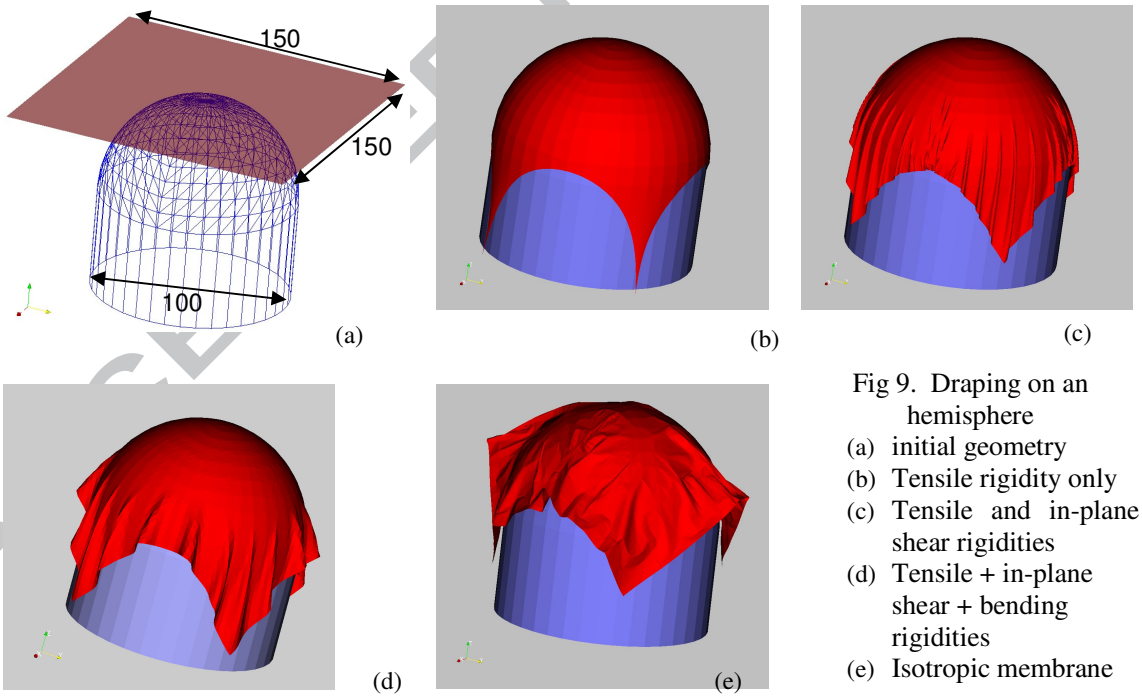

Fig 9. Draping on an hemisphere
(a) initial geometry
(b) Tensile rigidity only
(c) Tensile and in-plane shear rigidities
(d) Tensile + in-plane shear + bending rigidities
(e) Isotropic membrane

The size of the wrinkles becomes larger when the bending stiffness increases. Finally Fig 9e presents the deformed shape obtained when the in-plane shear stiffness corresponds to the one of an isotropic material (i.e. fixed by the tensile stiffness in order to have the same

axial rigidity in all the directions). In this case the draping on the hemisphere is not possible. The drapability of textile reinforcements on a double curved surface needs weak in-plane shear stiffness.

5.3. Forming of an unbalanced fabric

The textile reinforcement formed in Fig. 10 is very unbalanced (see table 1). The experimental forming by a hemispherical punch has been performed at the University of Nottingham. [56]. A 6 kg ring was used as blank-holder avoiding reinforcement wrinkling in the curved zone (Fig. 10a). The experimental shape obtained after forming is shown in Fig 10e. In the warp direction (with the strongest rigidity) large fabric sliding is observed relatively to the die. On the contrary, in the weft direction (weak direction) no edge movement is depicted and the yarns are subjected to large stretch deformations.

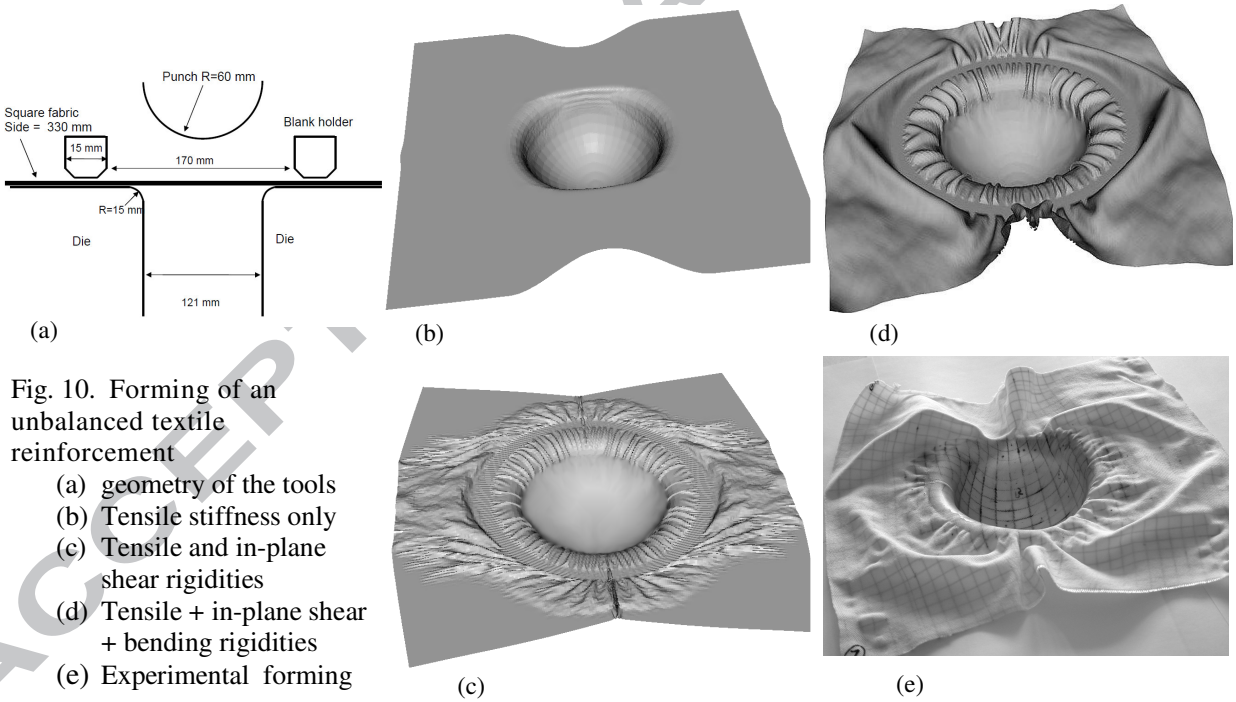

Fig. 10. Forming of an unbalanced textile reinforcement
(a) geometry of the tools
(b) Tensile stiffness only
(c) Tensile and in-plane shear rigidities
(d) Tensile + in-plane shear + bending rigidities
(e) Experimental forming

Near the central point of the preform, squares drawn on the fabric prior to forming become rectangles with a length/width ratio of 1.8 (see Fig 10e). The computed shapes after forming are shown Fig. 10b, c, d. In Fig. 10b, only the tensile stiffness is taken into account ((b) in equation 1). The dissymmetry of the shape in warp and weft direction is correctly obtained but there is no wrinkle. Fig. 10c shows the computed deformed shape when tension and in-

plane shear strain energies are considered (but no bending stiffness). A great number of small wrinkles are depicted. When the bending strain energy is added (Fig 10d), the wrinkles are much bigger and their shapes are in fairly good agreement with the experiment. It should be noted that, if the shape and number of the wrinkles are very different in the three simulations, the extension ratio at the centre of the hemisphere (l_{weft}/l_{warp} = 1.8) is correctly computed in the three cases. This ratio depends on the tensile rigidities that are taken into account in all three cases. In contrast a fishnet algorithm that ignores the mechanical properties would lead to the same deformation in both warp and weft directions and the ratio in the central part would remain equal to 1.

5.4. Forming with a cylindrical punch

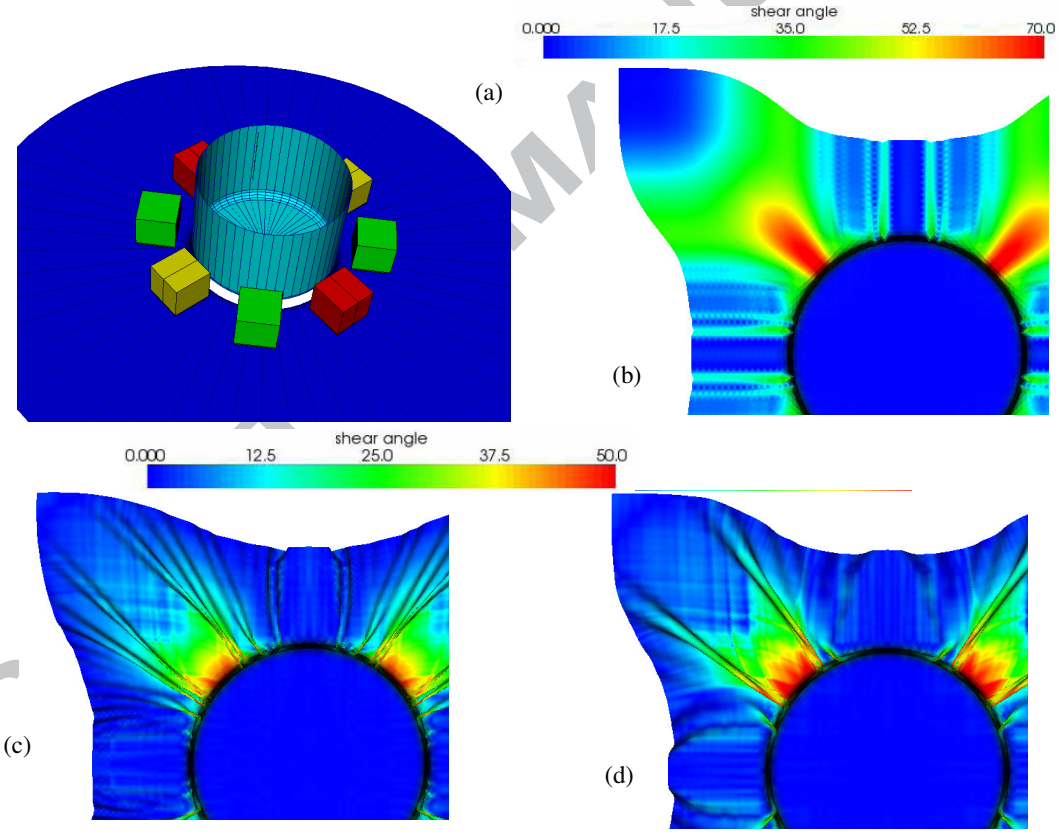

Fig. 11. Forming with a cylindrical punch. (a) geometry of the tools, (b) tensile stiffness only, (c) small bending stiffness, (d) higher bending stiffness

The simulation of the deep drawing of a woven reinforcement with a cylindrical punch is presented Fig. 11. There are height independent blank holders (Fig. 11a). Fig. 11b show the computed deformed shape of the reinforcement when only the tensile stiffness is taken into

account. There is no wrinkle and the computed shear angles are very large. They reach 70°. Figure 11c and 11d show the computed deformed shape when all the rigidities are considered in equation 1. The bending stiffness is 0.15 Nmm in Fig. 11c and 1.5 Nmm in Fig. 11d. There are many wrinkles in both cases especially between the blank holders. These wrinkles are less numerous and their size is larger (but moderately) when the bending stiffness increases.

5.5. Wrinkling and shear locking angle

Fig. 12, a textile reinforcement is shaped on a tetrahedron [57] thanks to strong forces on blank holders (similar to those presented in Fig. 11a). There is no wrinkle in the tetrahedral part of the preform, but there are many wrinkles in the plane zone. In zone A (Fig 12a), the shear angles are very large (close to 60°) and larger than the locking angle of the textile reinforcement (40°). This is possible thanks to strong tensions in the fabric due to the blank holders. On the other hand there are many wrinkles in the plane part of the preform where the shear angles are much smaller but where the tensions are weaker too. The simulation is in agreement with these points.

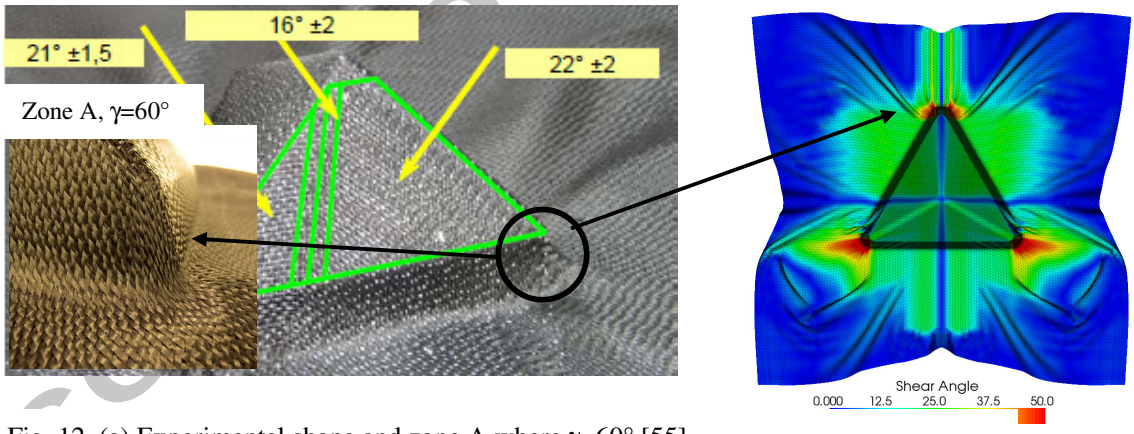

Fig. 12. (a) Experimental shape and zone A where γ=60° [55] (b) Numerical simulation

This example clearly shows that the comparison of the shear angle to the locking angle is not sufficient to predict wrinkling. The wrinkles are the result of a global mechanical problem (such as written in equation 1). Adequate tensions due to blank holders may lead to large shear angles without wrinkling.

6 – Conclusions

Wrinkling of textile reinforcement during forming processes has been analysed using a simplified form of the internal virtual work where the tension, in plane shear and bending parts are separated and related to load resultants on a unit woven cell. Taking one two or the three parts of internal virtual work into account, the influence of the in-plane shear and bending stiffnesses have been analysed. Forming double curved parts requires large shear angles that lead to an increase of the in-plane shear stiffness and consequently frequent wrinkling. Nevertheless the onset and growth of wrinkles is a global phenomenon that depends on the set of all strains and stiffnesses. Especially blank holders can create tensions that avoid wrinkling even for large shear angles.

Bending stiffness plays a main role in the shape of wrinkles. This rigidity must be taken into account in the simulations in order to verify that wrinkles do not extend to the useful part of the preform. This is not possible when the simulation is based on a membrane approach.

The quality of the wrinkle simulation depends on the mechanical properties that are taken into account. Some assumptions are made in the present work such as the independence of the in-plane shear and bending rigidities on the tension state. Similarly the twist term is neglected in bending stiffness. Some further experimental data on these points will be taken into account in the internal virtual work in order to improve the wrinkle simulations.

References

1. Advani SG. Flow and rheology in polymeric composites manufacturing. Elsevier, 1994.
2. Rudd CD., Long AC. Liquid Molding Technologies. Cambridge: Woodhead Pub. Lim., 1997.
3. De Luca P., Pickett AK. Numerical and experimental investigation of some press forming parameters of two fibre reinforced thermoplastics: APC2-AS4 and PEI-CETEX. Composites Part A 1998; 29: 101-110.
4. Hsiao SW., Kikuchi N. Numerical analysis and optimal design of composite thermoforming process. Comp. Meth Appl Mech Engrg 1999;177: 1-34.
5. Pickett AK. Review of finite element methods applied to manufacturing and failure prediction in composite structures. Applied Composite Material 2002; 9: 43-58.
6. Boisse P. Finite element analysis of composite forming. In: Long AC, editor. Composite forming technologies. Woodhead Publishing Limited, 2007.
7. Hill R., A general theory of uniqueness and stability in elastic–plastic solids. J Mech Phys Solids 1958; 8: 236-249.
8. Cao J., Boyce M. Wrinkle behavior of rectangular plates under lateral constraint. Int J of Solids Structures, 1997; 34 (2): 153-176.

9. Friedl N., Rammerstorfer FG., Fischer FD. Buckling of stretched strips. Comp & Struct 2000; 78 (1-3):185-190.
10. Cerda E., Mahadevan L. Geometry and Physics of Wrinkling. Physical review letters 2003; 90 (7): 074302-1-4.
11. Wang CT., Kinzel G., Altan T. Wrinkling criterion for an anisotropic shell with compound curvatures in sheet forming. Int J of Mech Sciences 1994; 36: 945-60.
12. Roddeman DG., Druker J., Oomens CWJ., Janssen JD. The wrinkling of thin membranes: part 1 – theory, part 2 – numerical analysis. Transactions of ASME 1987; 54: 884-892.
13. Prodromou AG., Chen J. On the relationship between shear angle and wrinkling of textile composite preforms. Composite Part A 1997; 28A:491-503.
14. Rozant O., Bourban PE., Manson JAE. Drapability of dry textile fabrics for stampable thermoplastic preforms. Composites: Part A 2000; 31: 1167-1177.
15. Potter K. Bias extension measurements on cross-plied unidirectional prepreg. Composites Part A 2002; 33: 63-73.
16. Lebrun G., Bureau MN., Denault J. Evaluation of bias-extension and picture-frame test for the measurement of shear properties of PP/glass commingled fabrics. Compos Struct 2003; 61: 341-52
17. Sharma S.B., Sutcliffe M.P.F., Chang S.H. Characterisation of material properties for draping of dry woven composite material. Composites Part A, 2003; 34:1167–1175.
18. B. Zhu, T.X. Yu, J. Teng, and X.M. Tao, Theoretical Modeling of Large Shear Deformation and Wrinkling of Plain Woven Composite, Journal of Composite Materials, 2009; 43: 125 - 138.
19. Long AC., Rudd CD. A simulation of reinforcement deformation during the production of preform for liquid moulding processes. IMechE J Eng Manuf 1994; 208: 269-278.
20. Wang J., Paton R., Page JR. The draping of woven fabric preforms and prepregs for production of polymer composite components. Composites Part A 1999; 30 (6):757-765.
21. Potluri P., Sharma S., Ramgulam R. Comprehensive drape modelling for moulding 3D textile preforms. Composites Part A 2001; 32 (10):1415-1424.
22. Skordos AA., Monroy Aceves C., Sutcliffe MPF. A simplified rate dependent model of forming and wrinkling of pre-impregnated woven composites. Composites: Part A 2007; 38: 1318-1330.
23. Cherouat A., Billoet JL. Mechanical and numerical modelling of composite manufacturing processes deep-drawing and laying-up of thin pre-impregnated woven fabrics, Journal of Materials Processing Technology 118 (2001) 460–471
24. H. Lin, J. Wang, A.C. Long, M.J. Clifford, P. Harrison, Predictive modelling for optimization of textile composite forming, Composites Science and Technology 67 (2007) 3242–3252
25. J. Lee, S. Hong, W. Yu, T. Kang, The effect of blank holder force on the stamp forming behaviour of non-crimp fabric with a chain stitch. Compos. Sci Tech (2007), 67(3-4):357-366
26. Kawabata S., Niwa M., Kawai H. The Finite Deformation Theory of Plain Weave Fabrics Part I: The Biaxial Deformation Theory. Journal of the Textile Institute 1973; 64(1): 21-46.
27. Buet-Gautier K., Boisse P. Experimental analysis and modeling of biaxial mechanical behavior of woven composite reinforcements. Experimental Mechanics 2001; 41 (3): 260-269.
28. Carvelli V., Corazza C., Poggi C. Mechanical modelling of monofilament technical textiles. Computational Materials Science 2008; 42: 679-691.
29. Willems A., Lomov SV., Verpoest I., Vandepitte D. Optical strain fields in shear and tensile testing of textile reinforcements. Composites Science and Technology 2008; 68: 807-819.
30. Peng XQ., Cao J., Chen J., Xue P., Lussier DS., Liu L. Experimental and numerical analysis on normalization of picture frame tests for composite materials. Compos Sci Tech 2004; 64: 11-21.
31. Harrison P., Clifford MJ., Long AC. Shear characterisation of viscous woven textile composites: a comparison between picture frame experiments. Compos Sci Tech 2004; 64: 1453-1465.
32. Potluri P., Perez Ciurezu DA., Ramgulam RB. Measurement of meso-scale shear deformations for modelling textile composites. Composites Part A 2006; 37: 303-314.
33. Lomov SV., Willems A., Verpoest I., Zhu Y., Barburski M., Stoilova Tz. Picture frame test of woven composite reinforcements with a full-field strain registration. Textile Research Journal 2006; 76 (3): 243-252.

34. Launay J., Hivet G., Duong AV., Boisse P. Experimental analysis of the influence of tensions on in plane shear behaviour of woven composite reinforcements. Compos Sci Tech 2008; 68: 506-515.
35. Lomov S., Boisse P., Deluycker E., Morestin F., Vanclooster K., Vandepitte D., Verpoest I., Willems A. Full field strain measurements in textile deformability studies. Composites: Part A 2008; 39: 1232-1244.
36. Cao J., Akkerman R., Boisse P., Chen J. et al. Characterization of Mechanical Behavior of Woven Fabrics: Experimental Methods and Benchmark Results. Composites Part A 2008; 39: 1037-1053.
37. Kawabata S. The Standardization and Analysis of Hand Evaluation. Osaka: The Textile Machinery Society of Japan, 1986.
38. Lahey TJ., Heppler GR. Mechanical Modeling of Fabrics in Bending. ASME Journal of Applied Mechanics 2004; 71: 32-40.
39. de Bilbao E, Soulat D, Hivet G, Gasser A., Experimental Study of Bending Behaviour of Reinforcements, Experimental Mechanics (2010) 50:333–351
40. Dong L., Lekakou C., Bader MG. Processing of composites: simulations of the draping of fabrics with updated material behaviour law. Journal of Composite Materials 2001; 35: 138-163.
41. W. Yu, P. Harrison, A. Long. Finite element forming simulation for non-crimp fabrics using a non-orthogonal constitutive equation, Composites: Part A 36 (2005) 1079–1093
42. Peng X., Cao J. A continuum mechanics-based non-orthogonal constitutive model for woven composite fabrics. Composites Part A 2005; 36: 859-874.
43. Ten Thije RHW., Akkerman R., Huetink J. Large deformation simulation of anisotropic material using an updated Lagrangian finite element method. Comp meth in appl mech and eng 2007; 196 (33-34): 3141-3150.
44. Hamila N. Simulation de la mise en forme des renforts composites mono et multiplis. PhD thesis, Université de Lyon, 2007.
45. Hamila N., Boisse P., Sabourin F., Brunet M. A semi-discrete shell finite element for textile composite reinforcement forming simulation. Int J Numerical Methods in Engineering 2009; 79: 1443-1466.
46. Lomov SV., Verpoest I. Model of shear of woven fabric and parametric description of shear resistance of glass woven reinforcements. Compos. Science and Technology 2006; 66: 919-933.
47. Duong AV. Etude experimentale du comportement mecanique de renforts composites tisses lors de la mise en forme sur geometries non developpables. PhD thesis, University of Orléans, 2008.
48. Peirce FT. The geometry of cloth structure. The Journal of the Textile Institute 1937; 28: 45-96.
49. ASTM Standard test method for stiffness of fabrics-ch. D1388-96. American S. for Testing 2002
50. Zienkiewicz OC., Taylor RL. The finite element method, vol. 2: Solid Mechanics. Oxford: Butterworth, Heineman, 2000.
51. Belytschko T. An overview of semidiscretisation and time integration procedures. In: Belytschko T, Hughes TJR, editors, Computation Methods for Transient Analysis. Amsterdam: Elsevier, 1983.
52. Onate E., Zarate F. Rotation-free triangular plate and shell elements. Int J for Num Meth in Eng 2000; 47: 557-603.
53. Sabourin F., Brunet M. Detailed formulation of the rotation-free triangular element “S3” for general purpose shell analysis. Engineering computations 2006; 23 (5): 469-502.
54. Yu X., Cartwright B., McGuckin D., Ye L., and Mai Y. W.. Intra-ply shear locking in finite element analyses of woven fabric forming processes. Compos Part A-Appl S, 2006, 37:790–803
55. ten Thije H.W., Akkerman R., Solutions to intra-ply shear locking in finite element analyses of fibre reinforced materials, Compos Part A-Appl S, 2008 ; 39 (7), 1167-1176.
56. Daniel JL., Soulat D., Dumont F., Zouari B., Boisse P., Long AC. Forming simulation of very unbalanced woven composite reinforcements. Int J of Forming Processes 2003; 6 (3-4): 465-480
57. D. Soulat, S. Allaoui, S. Chatel, Experimental device for the preforming step of the rtm process, Int J Mater Form (2009) Vol. 2 Suppl 1:181–184